GAMM-Mitt. **30**, No. 1, 44 – 74 (2007)

Boundary Perturbation Methods for Water Waves

David P. Nicholls *

Department of Mathematics, Statistics, and Computer Science,
851 South Morgan Street
University of Illinois at Chicago
Chicago, IL 60607

Key words Water waves, free–surface fluid flows, ideal fluid flows, boundary perturbation methods, spectral methods.
MSC (2000) 76B15, 76B07, 65M70, 65N35, 35Q35, 35J05

The most successful equations for the modeling of ocean wave phenomena are the free–surface Euler equations. Their solutions accurately approximate a wide range of physical problems from open–ocean transport of pollutants, to the forces exerted upon oil platforms by rogue waves, to shoaling and breaking of waves in nearshore regions. These equations provide numerous challenges for theoreticians and practitioners alike as they couple the difficulties of a free boundary problem with the subtle balancing of nonlinearity and dispersion in the absence of dissipation. In this paper we give an overview of, what we term, "Boundary Perturbation" methods for the analysis and numerical simulation of this "water wave problem." Due to our own research interests this review is focused upon the numerical simulation of traveling water waves, however, the extensive literature on the initial value problem and additional theoretical developments are also briefly discussed.

1 Introduction

The most successful equations for the modeling of ocean wave phenomena are the free–surface Euler equations. Their solutions accurately approximate a wide range of physical problems from open–ocean transport of pollutants, to the forces exerted upon oil platforms by rogue waves, to shoaling and breaking of waves in nearshore regions. These equations provide numerous challenges for theoreticians and practitioners alike as they couple the difficulties of a free boundary problem with the subtle balancing of nonlinearity and dispersion in the absence of dissipation. In this paper we give an overview of, what we term, "Boundary Perturbation" methods for the analysis and numerical simulation of this "water wave problem." Due to our own research interests this review is focused upon the numerical simulation of traveling water waves, however, the extensive literature on the initial value problem and additional theoretical developments are also briefly discussed.

In addition to Boundary Perturbation (BP) methods, a wide array of other techniques have been applied to the analysis of the Euler equations. After the early work on the linearized problem (see Lamb [43] for a complete discussion), the first successful and sustained effort to

* Corresponding author: e-mail: nicholls@math.uic.edu, Phone: (312) 413-1641, Fax: (312) 996-1491

capture *nonlinear* effects was probably the derivation and analysis of the long–wave Boussinesq and Korteweg–de Vries (KdV) equations for the two dimensional (one vertical and one horizontal) problem. For a complete history of the derivation of these and other equations, and for a detailed account of the Inverse Scattering method for the solution of these completely integrable equations, see, e.g., the monograph of Ablowitz & Segur [1]. Another avenue of research on water waves has been built upon the close connection between the two–dimensional Euler equations and complex analysis [43]. Subsequently, the tools of harmonic analysis and dynamical systems have been brought to bear on the problem for both theoretical analysis and numerical simulations.

Regarding numerical simulation, there is a vast literature concerning free–surface fluid flows. For these flows, attention has focused on boundary integral/element methods (BIM/BEM) and "high–order spectral" (HOS) methods. Both approaches posit unknown *surface* quantities and, due to this reduction in dimension, they are generally preferred to volumetric methods. In fact, for the two–dimensional problem almost all research has been focused on BIM due to this dimension–reducing property coupled with the convenient complex variables formulation and the availability of spectrally accurate quadrature rules. However, in three dimensions, the lack of a complex variables analogy and the difficulty of devising high–order quadratures has meant that a wide variety of methods have been analyzed. A comprehensive overview of the field up to the mid–1990's is given in Tsai & Yue [80]; notable among recent contributions are the BIM/BEM of Beale [4]; Grilli, Guyenne, and Dias [35]; Xue, Xu, Liu, and Yue [85]; and Liu, Xue, and Yue [46].

For traveling free–surface flows, Dias and Kharif [30] provide a thorough overview of much of the current theory and numerics. Of particular interest for the simulation of the full Euler equations are: Schwartz [75] who studied two–dimensional traveling patterns via complex variable theory, the BIM of Schwartz & Vanden-Broeck [76], and the three–dimensional HOS simulations of Rienecker and Fenton [69]; Meiron, Saffman, and Yuen [48]; Roberts and Schwartz [72]; Saffman and Yuen [73]; and Bryant [11].

Regarding Boundary Perturbation methods, they typically fall into one of two categories: Those that directly simulate the Euler equations (where the irregular, moving boundary is viewed as a perturbation of the quiescent state), and those that consider the Hamiltonian reformulation of Zakharov [86] (and perturb surface integral operators such as the "Dirichlet–Neumann operator," see § 2.3). Among the former are the traveling wave computations of Roberts, Schwartz, & Marchant [72, 70, 71, 47], and Nicholls & Reitich [60, 61]. Among the latter, the initial value problem has been studied by Watson & West [81]; West, Brueckner, Janda, Milder, & Milton [82]; and Milder [49] using surface integral operators related to the Dirichlet–Neumann operator. On the other hand, Craig & Sulem [26]; Craig, Schanz, & Sulem [74, 25]; de la Llave & Panayotaros [29]; Guyenne & Nicholls [36]; and Craig, Guyenne, Hammack, Henderson, & Sulem [20] used the Dirichlet–Neumann operator directly. Regarding traveling waves, Zakharov's formulation has received the attention of Nicholls [51, 52], and Craig & Nicholls [24] who wished to model waveforms displayed in, e.g., the wave–tank experiments of Hammack, Henderson, and Segur [37, 38].

Regarding theoretical developments with Boundary Perturbations, Reeder & Shinbrot [64, 65, 68]; Craig & Nicholls [23]; and Nicholls & Reitich [60] have shown existence and analyticity properties of branches and surfaces of traveling wave solutions. For the initial value problem, Boundary Perturbations applied to the formulation of Zakharov have been very fruitful in the derivation of long–wave approximations of the Euler equations (Craig, Sulem, & Sulem

[15]; Craig & Groves [18]; Craig, Guyenne, Nicholls, & Sulem [22]; and Craig, Guyenne, & Kalisch [21]), and the examination of integrability properties of the Euler equations (Craig & Worfolk [27]; Craig & Groves [19]; and Craig [17]).

The organization of the paper is as follows: In § 2 we recall the Euler equations of free–surface ideal fluid mechanics and, in particular, in § 2.1 the equations for the initial value problem and in § 2.2 the equations for the traveling wave problem. In § 2.3 we present the surface integral formulation of Zakharov [86], and, following Craig & Sulem [26], introduce the Dirichlet–Neumann operator to the water wave equations. In sections § 2.4, § 2.5, and § 2.6 we recall the "Operator Expansions," "Field Expansions," and "Transformed Field Expansions" Boundary Perturbation methods for computing the Dirichlet–Neumann operator. In § 3 we discuss Boundary Perturbation techniques and results for the initial value problem, while in § 4 we do the same for the traveling wave problem. Finally, in § 5 we present a novel, rapid and stable method for the computation of Dirichlet–Neumann operators which we advocate as a new and important direction in the development of Boundary Perturbation methods for not only the Euler equations, but also other free boundary and boundary value problems. In § 5.3 we present some preliminary numerical results to substantiate our claims.

2 Governing Equations

The Euler equations of free–surface fluid mechanics [43] constitute a highly successful model for ocean wave phenomena. In this section we state these equations, both for evolving and traveling waveforms, and recall their reformulation, due to Zakharov [86], as a Hamiltonian system in terms of *boundary* quantities. We follow Craig & Sulem's [26] observation that to make this formulation completely *explicit* one can introduce a "Dirichlet–Neumann operator," and then we describe three Boundary Perturbation algorithms for the numerical simulation of this operator.

2.1 The Initial Value Problem

Consider a d–dimensional ($d = 2, 3$) ideal (inviscid, irrotational, incompressible) fluid occupying the domain

$$S_{h,\eta} := \{(x, y) \in \mathbf{R}^{d-1} \times \mathbf{R} \mid -h < y < \eta(x, t)\},$$

meant to represent a fluid of mean depth h (which can be infinite) with time dependent free surface η. The irrotational and incompressible nature of the flow dictates that the fluid velocity inside $S_{h,\eta}$ can be expressed as the gradient of a potential, $u = \nabla\varphi$. The Euler equations govern the evolution of the potential and the surface shape under the effects of gravity and surface tension by:

$$\Delta\varphi = 0 \qquad \text{in } S_{h,\eta} \tag{1a}$$

$$\partial_y\varphi = 0 \qquad \text{at } y = -h \tag{1b}$$

$$\partial_t\varphi + \frac{1}{2}\left|\nabla\varphi\right|^2 + g\eta - \sigma\kappa(\eta) = 0 \qquad \text{at } y = \eta \tag{1c}$$

$$-\partial_t\eta + \partial_y\varphi - \nabla_x\eta \cdot \nabla_x\varphi = 0 \qquad \text{at } y = \eta, \tag{1d}$$

where g and σ are the constants of gravity and capillarity, respectively, and κ is the curvature:

$$\kappa(\eta) := \mathrm{div}_x \left[\frac{\nabla_x \eta}{\sqrt{1 + |\nabla_x \eta|^2}} \right].$$

The well–posedness theory of these equations is highly non–trivial which can be demonstrated by an inspection of the linearization of (1) about the quiescent state ($\eta = \varphi = 0$). The linearized solutions satisfy

$$\begin{aligned}
&\Delta\bar{\varphi} = 0 && \text{in } S_{h,0} \\
&\partial_y \bar{\varphi} = 0 && \text{at } y = -h \\
&\partial_t \bar{\varphi} + [g - \sigma\Delta_x]\bar{\eta} = 0 && \text{at } y = 0 \\
&-\partial_t \bar{\eta} + \partial_y \bar{\varphi} = 0 && \text{at } y = 0.
\end{aligned}$$

Consider the classical, horizontally periodic boundary conditions (characterized by period lattice $\Gamma \subset \mathbf{R}^{d-1}$ and conjugate lattice Γ', i.e. wavenumbers), then the solutions can be written as

$$\bar{\varphi}(x,y,t) = \sum_{k\in\Gamma'} a_k(t) \frac{\cosh(|k|\,(y+h))}{\cosh(|k|\,h)} e^{ik\cdot x}, \quad \bar{\eta}(x,t) = \sum_{k\in\Gamma'} d_k(t) e^{ik\cdot x},$$

where

$$\begin{pmatrix} a_k(t) \\ d_k(t) \end{pmatrix} = \Phi_k(t) \begin{pmatrix} a_k(0) \\ d_k(0) \end{pmatrix},$$

and the k–th block of the semi–group, Φ, is given, for $k \neq 0$, by

$$\begin{aligned}
&\Phi_k(t) := \begin{pmatrix} \cos(\omega_k t) & \alpha_k \sin(\omega_k t) \\ -(1/\alpha_k)\sin(\omega_k t) & \cos(\omega_k t) \end{pmatrix}, \\
&\omega_k := \sqrt{(g + \sigma\,|k|^2)\,|k| \tanh(h\,|k|)}, \quad \alpha_k := (g + \sigma\,|k|^2)/\omega_k.
\end{aligned}$$

The weakly dispersive nature of the operator Φ, particularly acute when $\sigma = 0$, coupled to the difficulties of the free–boundary formulation of (1) are precisely why its well–posedness theory is so challenging. However, significant progress has been made using the tools of integral equations and complex analysis by Reeder & Shinbrot [77, 66, 67], Kano & Nishida [40, 41], Craig [16], and Wu [83, 84]. To the author's knowledge the most general and complete result on well–posedness for the water wave problem is that of Lannes [44] who shows, for arbitrary depth and dimension (using the same method of proof), that the problem is well–posed for initial data in the Sobolev class H^s for $s > M$, $M = M(d)$.

2.2 Traveling Waves

A distinguished class of solutions to (1) are those translating without change in form with velocity $c \in \mathbf{R}^{d-1}$, i.e. the traveling waves. Traveling wave solutions of (1) must satisfy

$$\Delta\varphi = 0 \qquad \text{in } S_{h,\eta} \tag{2a}$$
$$\partial_y\varphi = 0 \qquad \text{at } y = -h \tag{2b}$$
$$[c\cdot\nabla_x]\varphi + \frac{1}{2}\left|\nabla\varphi\right|^2 + g\eta - \sigma\kappa(\eta) = 0 \qquad \text{at } y = \eta \tag{2c}$$
$$-[c\cdot\nabla_x]\eta + \partial_y\varphi - \nabla_x\eta\cdot\nabla_x\varphi = 0 \qquad \text{at } y = \eta. \tag{2d}$$

Using bifurcation theory, several general theorems on existence and smoothness of traveling wave solutions can be proven with the velocity c as the bifurcation parameter(s). Again, solutions of the linearized equations give valuable insights into both the character of solutions and the challenges present in establishing rigorous theorems. The linearized version of (2) is:

$$\Delta\tilde{\varphi} = 0 \qquad \text{in } S_{h,0} \tag{3a}$$
$$\partial_y\tilde{\varphi} = 0 \qquad \text{at } y = -h \tag{3b}$$
$$[c\cdot\nabla_x]\tilde{\varphi} + (g - \sigma\Delta_x)\tilde{\eta} = 0 \qquad \text{at } y = 0 \tag{3c}$$
$$-[c\cdot\nabla_x]\tilde{\eta} + \partial_y\tilde{\varphi} = 0 \qquad \text{at } y = 0. \tag{3d}$$

Solutions of (3a) & (3b) can be written, again for periodic boundary conditions, as

$$\tilde{\varphi}(x,y) = \sum_{k\in\Gamma'}\tilde{a}_k\frac{\cosh(|k|\,(y+h))}{\cosh(|k|\,h)}e^{ik\cdot x}, \quad \tilde{\eta}(x) = \sum_{k\in\Gamma'}\tilde{d}_k e^{ik\cdot x},$$

while (3c) & (3d) mandate that, for $k \neq 0$,

$$A_k\begin{pmatrix}\tilde{a}_k\\ \tilde{d}_k\end{pmatrix} := \begin{pmatrix} ic\cdot k & g+\sigma\left|k\right|^2 \\ |k|\tanh(h\,|k|) & -ic\cdot k\end{pmatrix}\begin{pmatrix}\tilde{a}_k\\ \tilde{d}_k\end{pmatrix} = 0.$$

Clearly, the determinant function

$$\Lambda_\sigma(c,k) := (c\cdot k)^2 - (g+\sigma\left|k\right|^2)\,|k|\tanh(h\,|k|) = (c\cdot k)^2 - \omega_k^2$$

plays a crucial role in the analysis, and for c and k such that $\Lambda_\sigma(c,k) \neq 0$, only *trivial* solutions, $\tilde{a}_k = \tilde{d}_k = 0$, exist. To find *non–trivial* solutions bifurcating from this trivial branch of solutions we select, for each $k_1 \in \Gamma'$, the unique (up to sign) velocity c_1 such that

$$\Lambda_\sigma(c_1,k_1) = 0,$$

which gives rise to solutions of (3) of the form

$$\tilde{\eta}(x) = \rho_1(c_1k_1)\cos(k_1x+\theta_1) \tag{4a}$$
$$\tilde{\varphi}(x,y) = \rho_1(g+\sigma k_1^2)\frac{\cosh(|k_1|\,(y+h))}{\cosh(|k_1|\,h)}\sin(k_1x+\theta_1), \tag{4b}$$

where, after a suitable translation, we can set $\theta_1 = 0$.

The bifurcation theoretic strategy to finding solutions of (2) is to seek *nonlinear* solutions near these *linear* solutions, (4). These results depend crucially on the dimension, d, and the presence or absence of surface tension, σ. For two–dimensional configurations ($d = 2$) there is a *unique* (up to sign) c_1 for each $k_1 \in \Gamma'$ such that $\Lambda_\sigma(c_1, k_1) = 0$. Without surface tension this is a problem of simple bifurcation [28] and was resolved in the pioneering papers of Levi–Civita [45] (infinite depth) and Struik [79] (finite depth). For two dimensional problems with surface tension this is, again, typically simple bifurcation, however, the phenomenon of *resonance* can arise if, for a fixed c_1, another wavenumber, $k_2 \in \Gamma'$, satisfies $\Lambda_\sigma(c_1, k_2) = 0$. For these "Wilton ripples" the analysis of Reeder & Shinbrot has been developed [68, 64].

The three–dimensional case is more complicated and, consequently, more interesting. First of all, the solution set $\Lambda_\sigma(c_1, k_1) = 0$ for a given $k_1 \in \Gamma'$ is now a *line* (up to sign) in the space of velocities so that the null space is infinite dimensional, though characterized by a single parameter. To identify a single solution from which to bifurcate, we choose a second, linearly independent, wavenumber $k_2 \in \Gamma'$ and find the unique (up to sign) velocity c_0 such that

$$\Lambda_\sigma(c_0, k_1) = 0, \quad \Lambda_\sigma(c_0, k_2) = 0. \tag{5}$$

From this velocity bifurcates a *surface* of solutions with *linear* behavior

$$\tilde{\eta}(x) = \rho_1(c_0 \cdot k_1)\cos(k_1 \cdot x + \theta_1) + \rho_2(c_0 \cdot k_2)\cos(k_2 \cdot x + \theta_2) \tag{6a}$$

$$\begin{aligned}\tilde{\varphi}(x,y) = {} & \rho_1(g + \sigma\,|k_1|^2)\frac{\cosh(|k_1|\,(y+h))}{\cosh(|k_1|\,h)}\sin(k_1 \cdot x + \theta_1) + \\ & + \rho_2(g + \sigma\,|k_2|^2)\frac{\cosh(|k_2|\,(y+h))}{\cosh(|k_2|\,h)}\sin(k_2 \cdot x + \theta_2),\end{aligned} \tag{6b}$$

where we can, once again, set $\theta_1 = \theta_2 = 0$ upon a suitable translation. Generically, for a c_0 which solves (5), if $k \in \Gamma'$ is not equal to a multiple of k_1 or k_2, then $\Lambda_\sigma(c_0, k) \neq 0$ and we have a (straightforward but non–trivial) generalization of simple bifurcation [65, 23, 60]. However, for any value of $\sigma \geq 0$ there is the possibility of additional wavenumbers $k_3, \ldots, k_p$ such that $\Lambda_\sigma(c_0, k_j) = 0$. Again, this is a phenomenon of resonance which greatly complicates theoretical results and, in three dimensions, is potentially stronger *without* surface tension than with it. By this we mean that, for $\sigma > 0$, p must be finite, while for $\sigma = 0$ we may encounter $p = \infty$ or, equally badly, $\Lambda_\sigma \ll 1$ for infinitely many k_j. Please see [23] for a complete discussion of these issues involving "small divisors."

From the solutions (6) the analysis of Reeder & Shinbrot [65], Craig & Nicholls [23], and Nicholls & Reitich [60] all proceed. Reeder & Shinbrot [65] demonstrated the existence and parametric analyticity of branches of capillary–gravity waves in the absence of resonance, while Craig & Nicholls [23] constructed bifurcation surfaces in the presence of "finite" resonance ($p < \infty$) with capillarity. Nicholls & Reitich [60] also investigated capillary–gravity waves (without resonance) to show *joint* parametric and spatial analyticity of wave profiles using a method which suggests a rapid, high–order, stable numerical method; this method was implemented and discussed in [61].

2.3 A Surface Integral Formulation and the Dirichlet–Neumann Operator

A simplification and reduction in dimension can be achieved for the water wave problem upon the realization that, given the surface deformation $\eta(x,t)$ and the Dirichlet trace of the potential at the surface $\xi(x,t)$, the full potential, $\varphi(x,y,t)$, can be recovered anywhere inside the domain $S_{h,\eta}$ via an appropriate integral formula [32]. Of course other surface quantities could be used, however, the Dirichlet data is distinguished by the discovery of Zakharov [86] that the pair (η,ξ) are, in fact, canonical variables in a Hamiltonian formulation of the water wave problem. The Hamiltonian presented by Zakharov is somewhat implicit in nature as the quantity ξ does not make an explicit appearance, however, this was rectified by Craig & Sulem [26] with the introduction of the Dirichlet–Neumann operator (DNO) to the formulation.

Of course DNO arise in a large number of diverse contexts (e.g. electromagnetics and acoustics, solid mechanics, very viscous flows, etc.). For this reason we keep the presentation quite general and note that advances and discoveries made in the context of water waves typically have implications for a wide range of fields. The "DNO Problem" which arises in ideal free–surface fluid mechanics is:

$$\Delta v = 0 \qquad\qquad y < \eta(x) \tag{7a}$$

$$v(x,\eta(x)) = \xi(x) \tag{7b}$$

$$\partial_y v \to 0 \qquad\qquad y \to -\infty, \tag{7c}$$

for a fluid of infinite depth. The case of finite depth is easily considered by replacing (7c) with

$$\partial_y v(x,-h) = 0, \tag{7d}$$

and we will, for simplicity, consider periodic boundary conditions. From this, the DNO, which maps Dirichlet data ξ to an (unnormalized) normal derivative of v at η, is defined by

$$G(\eta)[\xi] := \left[\nabla v \cdot N_\eta\right]_{y=\eta} = \left[\partial_y v - \nabla_x \eta \cdot \nabla_x v\right]_{y=\eta}, \tag{8}$$

where $N_\eta := (-\nabla_x \eta, 1)^T$. The choice of this particular normal is two–fold: First, as we shall see, it accommodates a particularly simple restatement of the water wave problem. Second, and more importantly, this DNO (with normal N_η) is self–adjoint which permits the implementation of a rapid Boundary Perturbation scheme for its numerical simulation.

In terms of this DNO the Hamiltonian for the water wave problem can be written [26]:

$$H(\eta,\xi) := \frac{1}{2}\int_{P(\Gamma)} \xi\, G(\eta)[\xi] + g\eta^2 + 2\sigma\left(\sqrt{1+\left|\nabla_x\eta\right|^2} - 1\right)\, dx. \tag{9}$$

Zakharov [86] showed that the initial value problem (1) can be written equivalently as

$$\partial_t \eta = \delta_\xi H(\eta,\xi), \quad \partial_t \xi = -\delta_\eta H(\eta,\xi),$$

where δ denotes functional variation, or (see [26]),

$$\partial_t \xi = -g\eta + \sigma \mathrm{div}_x \left[\frac{\nabla_x \eta}{\sqrt{1+|\nabla_x \eta|^2}} \right] - \frac{1}{2\left(1+|\nabla_x \eta|^2\right)} \Big\{ |\nabla_x \xi|^2 - (G(\eta)[\xi])^2 - 2G(\eta)[\xi] \nabla_x \xi \cdot \nabla_x \eta + |\nabla_x \xi|^2 |\nabla_x \eta|^2 - (\nabla_x \xi \cdot \nabla_x \eta)^2 \Big\} \tag{10a}$$

$$\partial_t \eta = G(\eta)[\xi]. \tag{10b}$$

In a similar fashion, the traveling wave equations (2) can be written [51] as

$$F_1(\eta, \xi, c) = 0, \quad F_2(\eta, \xi, c) = 0,$$

where

$$F_1(\eta, \xi, c) := [c \cdot \nabla_x]\xi + g\eta - \sigma \mathrm{div}_x \left[\frac{\nabla_x \eta}{\sqrt{1+|\nabla_x \eta|^2}} \right] + \frac{1}{2\left(1+|\nabla_x \eta|^2\right)} \Big\{ |\nabla_x \xi|^2 - (G(\eta)[\xi])^2 - 2G(\eta)[\xi] \nabla_x \xi \cdot \nabla_x \eta + |\nabla_x \xi|^2 |\nabla_x \eta|^2 - (\nabla_x \xi \cdot \nabla_x \eta)^2 \Big\} \tag{11a}$$

$$F_2(\eta, \xi, c) := -[c \cdot \nabla_x]\eta + G(\eta)[\xi]. \tag{11b}$$

While there are clearly many challenges, both analytical and numerical, to be addressed when using either (10) or (11) as a mathematical model, typically the greatest difficulty encountered arises from the DNO. On the theoretical side, due to the highly "non–standard" form of this order–one pseudodifferential operator, many useful PDE techniques (e.g. integration by parts) must be significantly altered or abandoned altogether. On the numerical side, the nontrivial shape of the domain coupled, again, with its non–standard form make standard treatments (e.g. finite difference and finite element methods) difficult to devise.

Despite this, a good deal is known about the properties of the DNO. Of particular interest, in the present context of Boundary Perturbation methods, is the following theorem which has been studied by many authors. To state a representative result precisely [57], we consider a boundary deformation of the form $\eta(x) = \varepsilon f(x)$ for some (small) parameter ε.

Theorem 2.1 *Given an integer $s \geq 0$, if $f \in C^{s+2}(P(\Gamma))$ and $\xi \in H^{s+3/2}(P(\Gamma))$ then the Taylor series*

$$G(\eta)[\xi] = G(\varepsilon f)[\xi] = \sum_{n=0}^{\infty} G_n(f)[\xi] \varepsilon^n, \tag{12}$$

converges strongly as an operator from $H^{s+3/2}(P(\Gamma))$ to $H^{s+1/2}(P(\Gamma))$ for ε sufficiently small. That is, there exist constants $K = K(s,d)$ and $C = C(s,d)$ such that

$$\|G_n(f)\|_{H^{s+1/2}} \leq K \|\xi\|_{H^{s+3/2}} B^n$$

for $B > C\,|f|_{C^{s+2}}$.

This result was first proven by Coifman & Meyer [14], using the theory of Calderón[12], for the case $d = 2$ when f is merely Lipschitz. This integral equation based approach was extended to three dimensions (for $f \in C^1$) by Craig, Schanz, and Sulem [25], and to arbitrary dimensions by Craig and Nicholls [23, 50]. Theorem 2.1 was proven by Nicholls & Reitich [55, 57] using a quite different method, based upon domain transformation, which inspired the numerical algorithm outlined in § 2.6. This method has been subsequently generalized to the Helmholtz equation by Nicholls & Nigam [53, 54] for applications arising in electromagnetics, and refined by Hu & Nicholls [39] to admit Lipschitz profiles in *arbitrary* dimensions, thereby extending the original result of Coifman & Meyer to higher dimension.

For numerical simulations the importance of the expansion (12) and Theorem 2.1 goes beyond the theoretical, and has quite important practical implications as they form the theoretical foundation for "Boundary Perturbation" (BP) techniques for computing DNO. In § 2.4, § 2.5, and § 2.6 we outline three algorithms for computing the G_n from (12), and we recall that these three BP algorithms for the computation of DNO have quite different properties in regard to numerical conditioning and computational complexity [56]. In § 5 we demonstrate how these can be combined into a new algorithm which possesses the strengths of both while ameliorating their weaknesses. Clearly, such an advance will have a huge impact on the numerical simulation of water waves in specific, and boundary value and free boundary problems in general.

2.4 Computation of Dirichlet–Neumann Operators: Operator Expansions

In the current exposition of Boundary Perturbation (BP) methods for computing DNO we will restrict ourselves to the setting of an ocean of infinite depth ($h = \infty$) and periodic boundary conditions. Of course formulas for the finite depth case ($h < \infty$) can also be derived (please see, e.g., [26, 55, 56]), but are somewhat more cumbersome.

The "Operator Expansions" (OE) strategy [82, 49, 26] to approximating DNO deals exclusively with the operator, G, and seeks its action on the basis functions $e^{ip\cdot x}$. The OE approach begins with the observation that

$$\varphi_p(x,y) := e^{ip\cdot x+|p|y} \tag{13}$$

satisfies (7a) & (7c). We now insert this "test function" into the definition of the DNO, (8),

$$G(\eta)\left[e^{ip\cdot x+|p|\eta}\right] = \left[|p| - \nabla_x\eta\cdot(ip)\right]e^{ip\cdot x+|p|\eta}.$$

Recalling that we have set $\eta = \varepsilon f$, and expanding the DNO and exponentials in powers of ε, we find:

$$\left(\sum_{n=0}^{\infty} G_n(f)\varepsilon^n\right)\left[\sum_{n=0}^{\infty}\frac{f^n}{n!}\,|p|^n\,e^{ip\cdot x}\right] = \left[|p| - \varepsilon\nabla_x f\cdot(ip)\right]\left[\sum_{n=0}^{\infty}\frac{f^n}{n!}\,|p|^n\,e^{ip\cdot x}\right].$$

At order zero in ε we discover that

$$G_0\left[e^{ip\cdot x}\right] = |p|\,e^{ip\cdot x},$$

and, provided that ξ can be represented by its Fourier series,

$$\xi(x) = \sum_{p\in\Gamma'} \hat{\xi}_p e^{ip\cdot x}, \tag{14}$$

define the following order–one Fourier multiplier

$$G_0[\xi] = G_0\left[\sum_{p\in\Gamma'} \hat{\xi}_p e^{ip\cdot x}\right] = \sum_{p\in\Gamma'} \hat{\xi}_p G_0\left[e^{ip\cdot x}\right] = \sum_{p\in\Gamma'} |p|\,\hat{\xi}_p e^{ip\cdot x} =: |D|\,\xi,$$

where $D := (1/i)\nabla_x$. Equating at order n in ε we obtain

$$G_n(f)\left[e^{ip\cdot x}\right] = \frac{f^n}{n!}\,|p|^{n+1}\,e^{ip\cdot x} - \frac{f^{n-1}}{(n-1)!}\nabla_x f\cdot(ip)\,|p|^{n-1}\,e^{ip\cdot x} - \sum_{l=0}^{n-1} G_l(f)\left[\frac{f^{n-l}}{(n-l)!}\,|p|^{n-l}\,e^{ip\cdot x}\right].$$

Using the Fourier multiplier notation $|D|$ and the fact that any sufficiently smooth ξ can be represented as a sum of complex exponentials we derive

$$G_n(f)[\xi] = \frac{f^n}{n!}\,|D|^{n+1}\,\xi - \frac{f^{n-1}}{(n-1)!}\nabla_x f\cdot\nabla_x\,|D|^{n-1}\,\xi - \sum_{l=0}^{n-1} G_l(f)\left[\frac{f^{n-l}}{(n-l)!}\,|D|^{n-l}\,\xi\right].$$

Finally, $|D|^2 = D\cdot D$ so that the first two terms can be combined to yield

$$G_n(f)[\xi] = D\cdot\left[\frac{f^n}{n!}D\,|D|^{n-1}\,\xi\right] - \sum_{l=0}^{n-1} G_l(f)\left[\frac{f^{n-l}}{(n-l)!}\,|D|^{n-l}\,\xi\right]. \tag{15}$$

Now (15) specifies a numerical algorithm once we define how the convolution products are computed; this, of course, is done via Fast Fourier Transform (FFT) acceleration. We now take up a careful accounting of the computational complexity of this method, and, for this, let us consider the $d = 2$ dimensional case with N_x Fourier modes and N perturbation orders. Clearly, the bottleneck in the computation of (15) is the term

$$X_{n,l} := G_l(f)\,[Y_{n,l}]\,,$$
$$Y_{n,l} := \frac{f^{n-l}}{(n-l)!}\,|D|^{n-l}\,\xi.$$

Of course, the cost of computing $Y_{n,l}$ (for (n,l) fixed) is $\mathcal{O}(N_x\log(N_x))$. However, the naive approach to forming the $X_{n,l}$ is to apply G_l to $Y_{n,l}$ from (15), and involves computing G_m *for all* $0\le m<l$. This scheme will have computational complexity $\mathcal{O}(N!)$, however, this enormous cost can be greatly reduced by *storing* the G_l as matrices (which act upon discretized

complex exponentials) and simply performing a matrix–vector product to find $X_{n,l}$. The cost of computing $G_n[e^{ip\cdot x}]$, given all G_l as matrices, is $\mathcal{O}(nN_x^2)$; this must be completed for N_x discrete complex exponentials and $0 \leq n \leq N$ orders so the *total* computational complexity is $\mathcal{O}(N^2N_x^3)$ while the storage is $\mathcal{O}(NN_x^2)$.

However, dramatic computational savings can be realized upon utilization of the self–adjointness property of the DNO. Noting the self–adjointness of D and $|D|$, we compute G_n^*, which equals G_n,

$$\begin{aligned} G_n(f)[\xi] &= G_n^*(f)[\xi] \\ &= (|D|^{n-1})^* D^* \cdot \left[\frac{f^n}{n!} D^* \xi\right] - \sum_{l=0}^{n-1} (|D|^{n-l})^* \frac{f^{n-l}}{(n-l)!} G_l^*(f)\,[\xi] \\ &= |D|^{n-1}\, D \cdot \left[\frac{f^n}{n!} D\xi\right] - \sum_{l=0}^{n-1} |D|^{n-l}\, \frac{f^{n-l}}{(n-l)!} G_l(f)\,[\xi]\,. \end{aligned} \tag{16}$$

Here we notice that the operator G_l always acts upon the *same* argument, ξ, thus we can store $G_l(f)[\xi]$, rather than the entire operator G_l, and compute G_n in time proportional to $\mathcal{O}(nN_x \log(N_x))$. Consequently the total complexity for all orders $0 \leq n \leq N$ is $\mathcal{O}(N^2 N_x \log(N_x))$, while the storage is merely $\mathcal{O}(NN_x)$.

2.5 Computation of Dirichlet–Neumann Operators: Field Expansions

In contrast to the Operator Expansions method, which works directly with the operator G, the "Field Expansions" (FE) approach [5, 31] begins with an expansion of the field v, which also depends analytically on ε [55, 57], and then produces the G_n from the expansion terms, v_n. To start,

$$v = v(x, y; \varepsilon) = \sum_{n=0}^{\infty} v_n(x, y)\varepsilon^n,$$

which, upon insertion into (7), demands that

$$\Delta v_n = 0 \qquad y < 0 \tag{17a}$$

$$v_n(x, 0) = H_n(x) \tag{17b}$$

$$\partial_y v_n \to 0 \qquad y \to -\infty, \tag{17c}$$

at every order n where

$$H_n(x) = \delta_{n,0}\xi(x) - \sum_{l=0}^{n-1} \frac{f^{n-l}}{(n-l)!} \partial_y^{n-l} v_l(x, 0),$$

and $\delta_{n,k}$ is the Kronecker delta. We recall that solutions v_n of (17a) & (17c) can be written as

$$v_n(x, y) = \sum_{p\in\Gamma'} a_{p,n} e^{ip\cdot x + |p|y}. \tag{18}$$

Given that $\xi(x)$ can be expressed by its Fourier series (14), (17b) delivers a recursion formula for the $a_{p,n}$:

$$a_{p,n} = \delta_{n,0}\hat{\xi}_p - \sum_{l=0}^{n-1}\sum_{q\in\Gamma'} C_{n-l,p-q}\,|q|^{n-l}\,a_{q,l}, \tag{19}$$

where the $C_{l,p}$ are defined by

$$\frac{f(x)^l}{l!} =: \sum_{p\in\Gamma'} C_{l,p}e^{ip\cdot x}.$$

Simply stated, the FE algorithm is (19) from which velocity potential information can be recovered, in particular the normal derivative at the surface, i.e. the DNO.

To compute the DNO we note that

$$\begin{aligned}\sum_{n=0}^{\infty} G_n(f)[\xi]\varepsilon^n = G(\varepsilon f)[\xi] &= \left[\partial_y v - (\varepsilon\nabla_x f)\nabla_x v\right]_{y=\varepsilon f}\\ &= \sum_{n=0}^{\infty}\sum_{p\in\Gamma'}(|p| - (\varepsilon\nabla_x f)\cdot(ip))a_{p,n}e^{ip\cdot x+|p|\varepsilon f}.\end{aligned}$$

From this we deduce that

$$\begin{aligned}G_n(f) = \sum_{l=0}^{n}\frac{f^{n-l}}{(n-l)!}\sum_{p\in\Gamma'}|p|^{n-l+1}\,a_{p,l}e^{ip\cdot x}\\ - \sum_{l=0}^{n-1}\frac{f^{n-l-1}}{(n-l-1)!}\nabla_x f\cdot\sum_{p\in\Gamma'}(ip)\,|p|^{n-l-1}\,a_{p,l}e^{ip\cdot x}.\end{aligned} \tag{20}$$

In using (19) & (20) for the numerical simulation of DNO the algorithm is completely determined once we specify that the convolutions are computed by FFT acceleration. Thus, for a simulation in $d = 2$ dimensions using N_x collocation points and N perturbation orders, the computational complexity both for (19) and (20) is $\mathcal{O}(N^2N_x\log(N_x))$ while the storage is $\mathcal{O}(NN_x)$.

2.6 Computation of Dirichlet–Neumann Operators: Transformed Field Expansions

While the Operator Expansions (16) and Field Expansions (19) & (20) algorithms each provide a rapid, easily implemented scheme for the simulation of DNO, they do have shortcomings. For a wide range of profiles, f, and sizes, ε, both algorithms provide robust, high–order results (see, e.g., [26, 5, 6, 7, 8, 9, 10]), however, as the roughness of f and/or the magnitude of ε is increased subtle cancellations in the OE and FE formalisms become apparent. This has been studied in great detail in the work of Nicholls & Reitich [55, 56, 57, 58, 59, 60, 61] and we recall some results and consequences of these studies in this section.

We note that neither the OE nor FE algorithms can be used to construct an analyticity proof for the DNO; as we have shown [55], such a strategy is thwarted by the cancellations

mentioned above which are destroyed upon use of standard PDE tools such as the triangle inequality in a Sobolev space. To overcome this numerical ill–conditioning we [55] sought out a *direct*, Boundary Perturbation proof for the analyticity of the DNO. We identified such a method by augmenting the FE approach with a preliminary transformation, producing the "Transformed Field Expansion" (TFE) algorithm. Before discussing the details, we restate the problem (7) on a truncated domain which not only allows for a unified statement of results for finite and infinite depth, but also delivers a much faster numerical algorithm.

Consider a hyperplane $y = -a$ strictly below the surface of the ocean ($a > |\eta|_{L^\infty}$), yet above the bottom of the ocean ($a < h$). Our goal is to equivalently state (7) on the *truncated* domain $S_{a,\eta}$. With this in mind we consider the augmented DNO problem

$$\begin{aligned}
&\Delta v = 0 && -a < y < \eta(x) && \text{(21a)}\\
&v(x,\eta(x)) = \xi(x) && && \text{(21b)}\\
&\partial_y v(x,-a) = \partial_y w(x,-a) && && \text{(21c)}\\
&v(x,-a) = w(x,-a) && && \text{(21d)}\\
&\Delta w = 0 && -h < y < -a && \text{(21e)}\\
&\partial_y w(x,-h) = 0, && && \text{(21f)}
\end{aligned}$$

where, clearly, the solutions (v, w) of (21) "match" those of (7) in that the v are equal on $S_{a,\eta}$, while $v = w$ on $-h < y < -a$. We now gather (21d)–(21f) as

$$\begin{aligned}
&\Delta w = 0 && -h < y < -a\\
&w(x,-a) = \zeta(x)\\
&\partial_y w(x,-h) = 0,
\end{aligned}$$

where $\zeta(x)$ stands for $v(x,-a)$, and notice that these equations have the exact solution

$$w(x,y) = \sum_{p\in\Gamma'} \hat{\zeta}_p \frac{\cosh(|p|\,(y+h))}{\cosh(|p|\,(h-a))} e^{ip\cdot x}.$$

Equation (21c) requires the normal derivative $\partial_y w$ thus we construct a second DNO:

$$\begin{aligned}
T[\zeta]: &= \partial_y w(x,-a)\\
&= \sum_{p\in\Gamma'} |p|\tanh(|p|\,(h-a))\hat{\zeta}_p e^{ip\cdot x}\\
&= |D|\tanh((h-a)\,|D|)\zeta,
\end{aligned}$$

and (21a)–(21c) can now be stated entirely in terms of v as

$$\begin{aligned}
&\Delta v = 0 && -a < y < \eta(x) && \text{(22a)}\\
&v(x,\eta(x)) = \xi(x) && && \text{(22b)}\\
&\partial_y v(x,-a) - T[v(x,-a)] = 0. && && \text{(22c)}
\end{aligned}$$

Equation (22) now provides the restatement of (7) on the truncated domain $S_{a,\eta}$ via a "transparent boundary condition" at $y = -a$ [60, 61].

We now discuss the TFE method for computing the G_n in the Taylor expansion of the DNO. Consider the (non–conformal) change of variables,

$$x' = x, \quad y' = a\left(\frac{y-\eta}{a+\eta}\right), \tag{23}$$

which maps $S_{a,\eta}$ to $S_{a,0}$. We find that the transformed potential

$$u(x', y') = v(x', ((a + \eta(x'))/a)y' + \eta(x')),$$

must satisfy

$$\begin{aligned}
&\Delta' u = F(x', y'; u) && -a < y' < 0\\
&u(x', 0) = \xi(x')\\
&\partial_{y'} u(x', -a) - T[u(x', -a)] = Q(x'; u),
\end{aligned}$$

where the precise forms of F and Q are given in [55, 56, 57]. In these papers it was shown that the transformed potential, u, is also analytic in ε so that we may make, upon dropping primes, the expansion

$$u(x, y; \varepsilon) = \sum_{n=0}^{\infty} u_n(x, y)\varepsilon^n.$$

It is not hard to show that the u_n must satisfy

$$\Delta u_n = F_n(x, y) \qquad -a < y < 0 \tag{24a}$$

$$u_n(x, 0) = \delta_{n,0}\xi(x) \tag{24b}$$

$$\partial_y u_n(x, -a) - T[u_n(x, -a)] = Q_n(x), \tag{24c}$$

where the F_n and Q_n are again given in [55, 56, 57]. From this the n–th term in the expansion of the DNO can be found from

$$\begin{aligned}
G_n(f)[\xi] = \partial_y u_n(x, 0) - \frac{f}{h} G_{n-1}(f)[\xi] - \nabla_x f \cdot \nabla_x u_{n-1}(x, 0)\\
- \frac{f}{h}\nabla_x f \cdot \nabla_x u_{n-2}(x, 0) + |\nabla_x f|^2 \partial_y u_{n-2}(x, 0).
\end{aligned}$$

Complete details with a full discussion of implementation issues and numerical results can be found in [56]. From this we recall that, in contrast to the OE and FE procedures, and due to the inhomogeneous nature of the Poisson equation (24a), we are unable to solve (24) without a discretization of the y–variable. We can partially ameliorate this difficulty with the use of a fast, Chebyshev spectral method [34, 13] at a cost $\mathcal{O}(N_y \log(N_y))$ per order n and wavenumber k, where N_y is the number of Chebyshev polynomials utilized. Also, with the domain truncated at $y = -a$ we can choose a quite small in the hope that N_y need not be chosen very large. However, the total execution time is $\mathcal{O}(NN_x \log(N_x)N_y \log(N_y))$ and the total storage is $\mathcal{O}(NN_xN_y)$.

Despite this disadvantaged operation count, as compared with other BP methods, the increased accuracy and stability of the TFE method renders it the most compelling option in many applications. We will return to these points in § 5 as they provide the impetus for one "future direction" we foresee in BP methods for water waves and other boundary value and free boundary problems: The combination of the FE and TFE algorithms to produce a rapid *and* stable high–order method.

3 Boundary Perturbation Methods for the Initial Value Problem

Several authors have investigated Boundary Perturbation techniques for the approximation of the water wave initial value problem (1). These generally fall into one of the two categories: Those that deal directly with the full Euler equations (1), and those that approximate the surface formulation (10) of Zakharov [86] and Craig & Sulem [26].

Examples of Boundary Perturbation approaches to (1) are the work of Fenton & Rienecker [33] who studied solitary wave interactions of the full Euler equations, and Dommermuth & Yue [31]. In these methods one assumes that the quantities η and φ depend analytically on the small parameter ε (representing the height/slope of the wave) and insert the Taylor expansions

$$\eta(x,t;\varepsilon) = \sum_{n=1}^{\infty} \eta_n(x,t)\varepsilon^n, \quad \varphi(x,y,t;\varepsilon) = \sum_{n=1}^{\infty} \varphi_n(x,y,t)\varepsilon^n,$$

directly into (1). These are then equated at orders of ε, and a modal expansion of the η_j and φ_j results in a set of time–dependent coefficients that must be evolved. For derivatives of η_j and *tangential* derivatives of φ_j this is straightforward, however, for normal derivatives of the velocity potential the modes are coupled in a complicated way. Of course this is to be expected as this operation is simply the DNO discussed in § 2.3.

Zakharov's Hamiltonian formulation of the water wave problem [86] was pursued by Watson & West [81], and West, Brueckner, Janda, Milder, and Milton [82] to produce a numerical algorithm based upon Boundary Perturbation of the Hamiltonian (9). While the language of the DNO was not used, the operators $|D|$ and convolutions (written as commutators) are clearly evident. Craig & Sulem [26], Schanz [74], and Guyenne & Nicholls [36] all use (10) as their starting point and approximate the DNO, rather than the Hamiltonian, by its truncation

$$G^N(\eta)[\xi] := \sum_{n=0}^{N} G_n(\eta)[\xi].$$

Craig & Sulem [26] considered the two–dimensional case in the absence of capillarity, while Schanz [74] generalized to three dimensions in the presence of surface tension. Guyenne & Nicholls [36] studied two–dimensional gravity waves over plane slopes (bathymetry) which required a generalization of the DNO to include bottom topography. Please see Smith [78]; Craig, Guyenne, Nicholls, and Sulem [22]; and Nicholls and Taber [63] for more details on this extension. Recently, Craig, Guyenne, Hammack, Henderson, and Sulem [20] used this approach to revisit the problem of solitary wave interactions and compared the results with those of wave–tank experiments. Finally, we point out the work of de la Llave & Panayotaros [29] on the simulation of gravity waves on the sphere. Of course, the water wave equations do not provide a useful model for the ocean on the surface of the earth, however, it is an interesting and non–trivial extension of this approach to spherical geometries.

4 Boundary Perturbation Methods for Traveling Waves

As we mentioned in the Introduction, with the availability of convenient and spectrally accurate integral equations methods, little effort has been expended upon the investigation of traveling two–dimensional water waves using Boundary Perturbation techniques (however, see [24] for some two–dimensional BP results). For this reason we will focus, for the rest of this section, upon the problem of simulating genuinely three–dimensional traveling waveforms. In this setting Boundary Perturbation methods have been applied to not only the original Euler equations (2), but also the surface formulation (11) and the transformed Euler equations (26).

In the case of the original Euler equations (2) the work of Roberts [70], Roberts & Peregrine [71], and Marchant & Roberts [47] is definitive in the absence of surface tension (it appears, however, that the subtleties of the existence theory for pure gravity waves in three dimensions was not properly appreciated by these authors, see § 2.2). We also note the closely related work of Roberts & Schwartz [72] which also considered the computation of three–dimensional traveling waves, but did not utilize a BP approach. All of these BP methods postulate Taylor expansions of the form

$$\eta(x;\varepsilon) = \sum_{n=1}^{\infty} \eta_n(x)\varepsilon^n, \quad \varphi(x,y;\varepsilon) = \sum_{n=1}^{\infty} \varphi_n(x,y)\varepsilon^n, \quad c(\varepsilon) = \sum_{n=0}^{\infty} c_n\varepsilon^n \tag{25}$$

and insert these directly into (2). Equating at orders of ε one recovers, at order one, the linear solutions (6) provided that c_0 satisfies (5) for two wavenumbers k_1 and k_2. At higher orders, the perturbative procedure delivers a linear inhomogeneous PDE to be solved for the unknowns $(\eta_n, \varphi_n, c_{n-1})$. The linear operator in this PDE is (3) which is, of course, singular precisely by the choice of c_0; however, the parameter c_{n-1} can be chosen to verify the associated solvability condition, and several parameterizations of the bifurcation curve are available which select a unique solution. We refer the interested reader to [60] for a complete specification of this method using the particular notations used in the present paper. Once again, the real issue with this method is the evaluation of normal derivatives of the velocity potential at the free surface. Roberts *et al* chose to implement an algorithm similar to that of the FE method presented in § 2.5, however, the details are complicated by the fact that one must evaluate these quantities not simply at a profile which depends *linearly* on ε ($\eta = \varepsilon f$) but rather in a *nonlinear*, though analytic, fashion, c.f. (25). Consequently, this algorithm has computational complexity $\mathcal{O}(N^3 N_1^2 N_2^2)$ for a simulation involving N perturbation orders and $N_1 \times N_2$ spatial collocation points. In addition, this method, much like the FE algorithm, is severely ill–conditioned for N large (please see [60, 61] for demonstrations).

Of course the conditioning properties of methods based on (11) depend strongly upon the implementation of the DNO: High–order numerics based upon OE and FE implementations will be rather unstable, while those using the TFE method will enjoy much greater stability, at perhaps a slightly higher computational cost (see § 2.4, § 2.5, and § 2.6). The computations of Nicholls [50, 51], and Craig & Nicholls [24] were based on an OE implementation of the DNO, but were performed at a relatively low perturbation order, $N = 5$. These simulations utilized Boundary Perturbations solely in the computation of the DNO and otherwise used numerical continuation [42, 2] to find solutions of (11) along the branch using a predictor–corrector algorithm.

In quite recent work, Nicholls & Reitich [61] numerically approximated the transformed recursions for traveling water waves derived in [60] using a Fourier/Chebyshev spectral method.

The derivation of these equations is quite similar to that presented in § 2.6 and, in fact, the change of variables (23) is identical. This transformation is applied to (2) (modified to include a "transparent boundary condition," c.f. (22)) and results, for the unknowns η, c, and the transformed potential

$$u(x', y') = \varphi(x', (a + \eta(x'))y'/a + \eta(x')),$$

in the following system of equations (upon dropping primes):

$$\Delta u = F(x, y; u) \qquad -a < y < 0 \tag{26a}$$
$$\partial_y u(x, -a) - Tu(x, -a) = J(x; u) \tag{26b}$$
$$[c_0 \cdot \nabla_x]\, u + [g - \sigma \Delta_x]\, \eta = Q(x; u) \qquad \text{at } y = 0 \tag{26c}$$
$$-[c_0 \cdot \nabla_x]\, \eta + \partial_y u = R(x; u) \qquad \text{at } y = 0, \tag{26d}$$

where the forms of F, J, Q, and R are given in [61].

Following the Field Expansions philosophy we posit the expansions

$$\eta(x; \varepsilon) = \sum_{n=1}^{\infty} \eta_n(x)\varepsilon^n, \quad \varphi(x, y; \varepsilon) = \sum_{n=1}^{\infty} \varphi_n(x, y)\varepsilon^n, \quad c(\varepsilon) = \sum_{n=0}^{\infty} c_n \varepsilon^n.$$

These (η_n, u_n, c_{n-1}) are governed by

$$\Delta u_n = F_n(x, y) \qquad -a < y < 0 \tag{27a}$$
$$\partial_y u_n(x, -a) - Tu_n(x, -a) = J_n(x) \tag{27b}$$
$$[c_0 \cdot \nabla_x]\, u_n + [g - \sigma \Delta_x]\, \eta_n = Q_n(x) - [c_{n-1} \cdot \nabla_x]\, u_1 \qquad \text{at } y = 0 \tag{27c}$$
$$-[c_0 \cdot \nabla_x]\, \eta_n + \partial_y u_n = R_n(x) + [c_{n-1} \cdot \nabla_x]\, \eta_1 \qquad \text{at } y = 0, \tag{27d}$$

where the F_n, J_n, Q_n, and R_n can be found in [61]. Here η_1 and u_1 are linear solutions (c.f. (6)) provided c_0 satisfies (5) and, again, the linear operator (3) appears on the left–hand side of (27). As with the approach of Roberts *et al* [70, 47], the velocity c_{n-1} is used to satisfy the solvability condition required by the singular nature of the system (27), while several parameterizations of the bifurcation curve can be given which produce a unique solution at every order; please see [61] for details.

On the theoretical side, Reeder & Shinbrot [68] proved the existence of solution branches to (26) and *parametric* (i.e. with respect to ε) analyticity using the perturbative approach outlined above. Their strategy required that not only $\sigma > 0$ but also the absence of resonance (see § 2.2). Craig & Nicholls [23] extended these results with an application of the Lyapunov–Schmidt theory to (11) and noted that solutions come in *surfaces* rather than simply branches. Their analysis still required $\sigma > 0$ but permitted "finite" resonance (provided that $p < \infty$, see § 2.2). Nicholls & Reitich [60] extended the method of Reeder & Shinbrot by not only verifying, quite directly, that solutions do come in surfaces, by making expansions of the form

$$\eta(x; \varepsilon_1, \varepsilon_2) = \sum_{n_1 + n_2 \geq 1} \eta_{n_1, n_2}(x) \varepsilon_1^{n_1} \varepsilon_2^{n_2},$$

but also by showing that the velocity potential and traveling wave surface are *jointly* analytic with respect to both parameters (ε_1, ε_2) and spatial variables (x, y).

On the computational side, Nicholls & Reitich [61] showed that the TFE recursions for water waves (27) could be converted into a rapid, high–order, stable numerical method for computing traveling water waves. Not only does this method enjoy the stability properties of the TFE method for DNO (as compared to the OE and FE implementations), but also, and in contrast to the situation for computing DNO, it has a *greatly reduced* operation count in comparison to the Roberts algorithm. In fact, we showed that the computational complexity is

$$\mathcal{O}(NN_1N_2\log(N_y)N_y + N^2N_1N_2N_y)$$

to be compared with $\mathcal{O}(N^3N_1^2N_2^2)$ for Roberts [70] and Marchant & Roberts [47]. With this efficiency and high–order stability we are now able to produce extremely accurate simulations of highly nonlinear waveforms as we now demonstrate.

For this we revisit the calculations of Nicholls & Reitich [61] and specialize to the geometry of the "short–crested waves" (SCW) [70]. A short–crested wave is a traveling waveform that is not only periodic in the direction of propagation, but also periodic in the orthogonal horizontal direction. The period in the propagation direction is set to $L/\sin(\theta)$ while the period in the orthogonal direction is $L/\cos(\theta)$. If we choose the x_1–axis as the direction of propagation and non–dimensionalize by setting $L = 2\pi$, the solutions will be periodic with respect to the lattice

$$\Gamma_\theta = \{\gamma = j_1 a + j_2 b \mid a = (2\pi)/\sin(\theta), b = (2\pi)/\cos(\theta); j_1, j_2 \in \mathbf{Z}\}, \tag{28}$$

i.e. $\eta(x+\gamma) = \eta(x)$ for all $\gamma \in \Gamma_\theta$. We also consider the case of water of infinite depth ($h = \infty$), and in all calculations the numerical parameters were set to $N_1 = N_2 = 64$ (Fourier modes in the horizontal directions), $N_y = 48$ (Chebyshev coefficients in the vertical direction), and $N = 31$ (perturbation orders).

For each of three values of $\theta = 45^o, 60^o, 75^o$ we selected two values of the parameter ε which were meant to prescribe "moderately nonlinear," and "highly nonlinear" profiles. We summarize these choices and our results in Table 1. Furthermore, in Figures 1–12 we reproduce plots of these solutions from [61]. From this it is easy to see how the waves become more nonlinear (with sharper, narrower crests and wider, shallower troughs) as ε is increased. Also, notice how the "shape" of the wave deforms from diamond–like to rectangular as θ is increased, in nice agreement with the experimental results of Hammack, Henderson, and Segur [37, 38].

5 Future Directions: Rapid and Stable High–Order Methods

As we have seen, Boundary Perturbation methods provide a fast, stable, and highly accurate method for the simulation of water waves. However, the stabilized methods we advocate here can be slightly disadvantaged in terms of computational complexity in comparison with other schemes (e.g. for the computation of DNO). One direction of future research is to address this concern with the development of methods with the speed of the FE recursions which retain the stability and accuracy properties of the TFE procedure. We now present a novel algorithm based upon the FE philosophy, but inspired by the success of the TFE scheme, to achieve precisely these requirements. For this discussion of "future directions" we restrict ourselves to the computation of DNO, however, it should be clear how to extend these ideas to more general situations.

Table 1 Summary of traveling wave calculations.

Figure	θ	ε	$\lvert\eta(x;\varepsilon)\rvert_{L^\infty}$	Plot Type
Figure 1	45^o	0.21	0.224997	Surface
Figure 2	45^o	0.43	0.487929	Surface
Figure 3	45^o	0.21	0.224997	Contour
Figure 4	45^o	0.43	0.487929	Contour
Figure 5	60^o	0.21	0.228521	Surface
Figure 6	60^o	0.42	0.491571	Surface
Figure 7	60^o	0.21	0.228521	Contour
Figure 8	60^o	0.42	0.491571	Contour
Figure 9	75^o	0.2	0.226086	Surface
Figure 10	75^o	0.41	0.542079	Surface
Figure 11	75^o	0.2	0.226086	Contour
Figure 12	75^o	0.41	0.542079	Contour

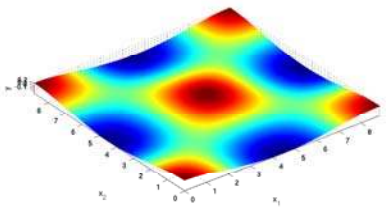

Fig. 1 Surface plot of ocean profile with $\theta = 45^o$ and $\varepsilon = 0.21$.

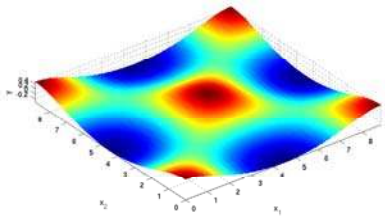

Fig. 2 Surface plot of ocean profile with $\theta = 45^o$ and $\varepsilon = 0.43$.

5.1 Stabilized Field Expansions

The success of the TFE method for computing DNO in a stable, high–order fashion is that the change of variables enforces that all derivatives be taken *inside* the problem domain. By contrast, the FE recursions require the differentiation of the field at $y = 0$ which is sometimes *across* the boundary of the problem domain. With this in mind we consider a number $b > |\eta|_{L^\infty}$ and the *family* of surfaces which are strictly *interior* to the domain,

$$\sigma_\delta(x;b) := (1-\delta)(-b) + \delta\eta(x) = -b + \delta(\eta(x)+b);$$

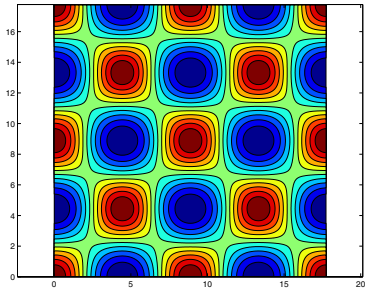

Fig. 3 Contour plot of ocean profile with $\theta = 45^o$ and $\varepsilon = 0.21$.

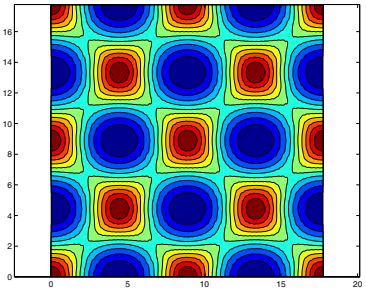

Fig. 4 Contour plot of ocean profile with $\theta = 45^o$ and $\varepsilon = 0.43$.

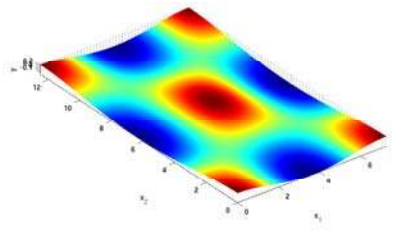

Fig. 5 Surface plot of ocean profile with $\theta = 60^o$ and $\varepsilon = 0.21$.

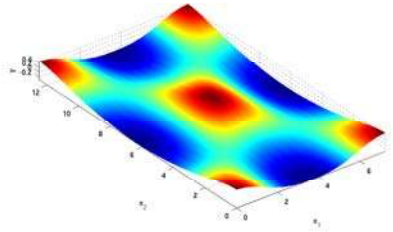

Fig. 6 Surface plot of ocean profile with $\theta = 60^o$ and $\varepsilon = 0.42$.

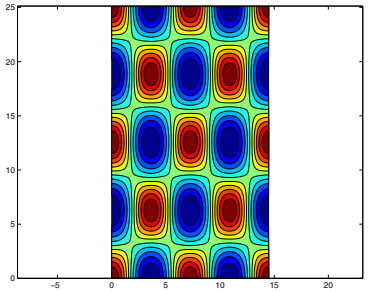

Fig. 7 Contour plot of ocean profile with $\theta = 60^o$ and $\varepsilon = 0.21$.

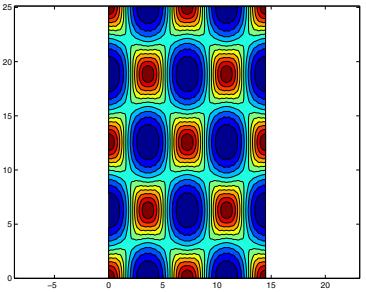

Fig. 8 Contour plot of ocean profile with $\theta = 60^o$ and $\varepsilon = 0.42$.

note that $\sigma_0 = -b$ and $\sigma_1 = g(x)$, i.e. σ_δ provides a homotopy from the hyperplane $y = -b$ to the ocean surface $y = \eta$. We will now consider δ as our expansion parameter and expand

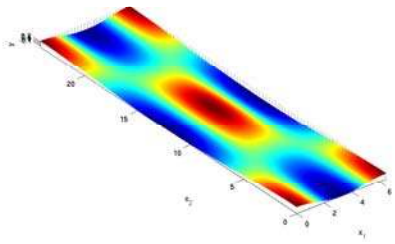

Fig. 9 Surface plot of ocean profile with $\theta = 75^o$ and $\varepsilon = 0.2$.

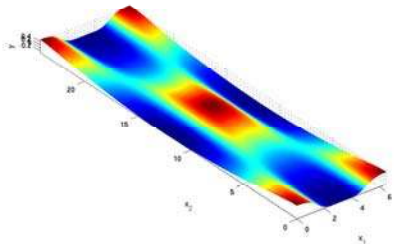

Fig. 10 Surface plot of ocean profile with $\theta = 75^o$ and $\varepsilon = 0.41$.

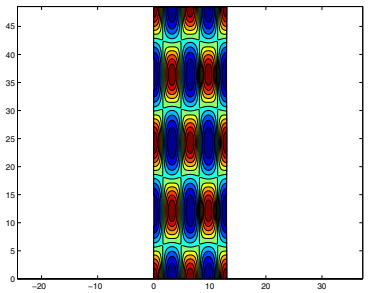

Fig. 11 Contour plot of ocean profile with $\theta = 75^o$ and $\varepsilon = 0.2$.

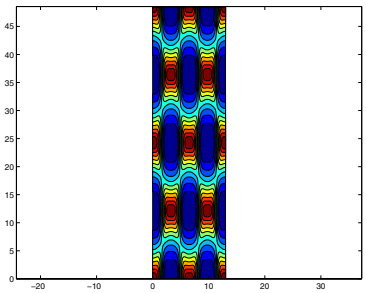

Fig. 12 Contour plot of ocean profile with $\theta = 75^o$ and $\varepsilon = 0.41$.

the field

$$v = v(x, y; \delta) = \sum_{n=0}^{\infty} v_n(x, y)\delta^n,$$

where, to find quantities at the ocean surface, we evaluate at $\delta = 1$. To find the v_n we look to (7) and note that v satisfies both Laplace's equation for $y < \sigma_\delta$, and equation (7c). The

Dirichlet condition (7b) implies

$$\begin{aligned}
\xi(x) &= v(x,\sigma_\delta;\delta)|_{\delta=1} \\
&= \left[\sum_{n=0}^{\infty} v_n(x,\sigma_\delta)\delta^n\right]_{\delta=1} \\
&= \left[\sum_{n=0}^{\infty} v_n(x,-b+\delta(\eta+b))\delta^n\right]_{\delta=1} \\
&= \left[\sum_{n=0}^{\infty}\left(\sum_{m=0}^{\infty}\frac{(\eta+b)^m}{m!}\partial_y^m v_n(x,-b)\delta^m\right)\delta^n\right]_{\delta=1} \\
&= \left[\sum_{n=0}^{\infty}\delta^n\sum_{l=0}^{n}\frac{(\eta+b)^{n-l}}{(n-l)!}\partial_y^{n-l}v_l(x,-b)\right]_{\delta=1}.
\end{aligned}$$

Therefore we can write the analogue of (17b):

$$v_n(x,-b) = \delta_{n,0}\xi(x) - \sum_{l=0}^{n-1}\frac{(\eta+b)^{n-l}}{(n-l)!}\partial_y^{n-l}v_l(x,-b).$$

Since v_n can be expressed as

$$v_n(x,y) = \sum_{p\in\Gamma'} d_{p,n}e^{ip\cdot x+|p|y},$$

c.f. (18), it is easy to show that

$$d_{p,n} = e^{|p|b}\left\{\delta_{n,0}\hat{\xi}_p - \sum_{l=0}^{n-1}\sum_{q\in\Gamma'}K_{n-l,p-q}e^{-|q|b}\,|q|^{n-l}\,d_{q,l}\right\}, \tag{29}$$

where the $K_{l,p}$ are defined by

$$\frac{(\eta+b)^l}{l!} =: \sum_{p\in\Gamma'}K_{l,p}e^{ip\cdot x}.$$

Defining the pseudodifferential operator S_D as

$$S_D[\psi] := \sum_{p\in\Gamma'}S_p\hat{\psi}_p e^{ip\cdot x} = \sum_{p\in\Gamma'}e^{-|p|b}\hat{\psi}_p e^{ip\cdot x},$$

and identifying its inverse

$$S_D^{-1}[\psi] = \sum_{p\in\Gamma'}S_p^{-1}\hat{\psi}_p e^{ip\cdot x} = \sum_{p\in\Gamma'}e^{|p|b}\hat{\psi}_p e^{ip\cdot x},$$

we rewrite (29) as

$$d_{p,n} = S_p^{-1}\left\{\delta_{n,0}\hat{\xi}_p - \sum_{l=0}^{n-1}\sum_{q\in\Gamma'}K_{n-l,p-q}S_q\,|q|^{n-l}\,d_{q,l}\right\}. \tag{30}$$

With this notation we point out some of the advantages and shortcomings of this "modified" Field Expansions method,(30). Clearly, the operator S_D is "infinitely smoothing" (mapping, for instance, L^2 functions to the class of real analytic functions) and we can hope that this operator will "smooth away" errors magnified by the order $(n-l)$ pseudodifferential operator $|D|^{n-l}$. However, the operator S_D^{-1} must also be applied and this will, at all scales, exponentially amplify truncation errors. To ameliorate this effect we introduce the modified operator B_D^F:

$$B_D^F[\psi] := \sum_{p\in\Gamma'} B_p^F \hat{\psi}_p e^{ip\cdot x}, \quad B_p^F := \begin{cases} e^{|p|b} & |p| \leq F \\ 0 & |p| > F \end{cases},$$

and now define the Stabilized Field Expansions (SFE) method as

$$d_{p,n} = B_p^F \left\{ \delta_{n,0}\hat{\xi}_p - \sum_{l=0}^{n-1} \sum_{q\in\Gamma'} K_{n-l,p-q} S_q \left|q\right|^{n-l} d_{q,l} \right\}. \tag{31}$$

In § 5.3 we will present some preliminary numerical results showing how this algorithm, combined with the ideas of § 5.2 on Dirichlet–Interior Derivative Operators, can give greatly enhanced numerical results, as compared to an FE implementation, with the same computational complexity.

5.2 Dirichlet–Interior Derivative Operators

Following the philosophy of [59], to compute the DNO we consider a family of "Dirichlet–Interior Derivative Operators" (DIDO) which evaluate the "normal derivative," $\nabla v \cdot N_\eta$, at the *interior* surface σ_δ introduced above. As discussed in [59], this operation should be largely free from the severe cancellations present in formulas (19) & (20) since no derivatives of the field are taken *across* the boundary $y = \eta(x)$. Of course, to compute the actual DNO we must evaluate at the surface $y = \eta(x)$, i.e. at $\delta = 1$.

We define our family of DIDO as

$$\tilde{G}(\delta)[\xi] := \left[\nabla v \cdot N_\eta\right]_{y=\sigma_\delta} = \left[\partial_y v - \nabla_x \eta \cdot \nabla_x v\right]_{y=\sigma_\delta},$$

for every $0 \leq \delta \leq 1$. To compute these DIDO we expand

$$\tilde{G}(\delta)[\xi] = \sum_{n=0}^{\infty} \tilde{G}_n[\xi]\delta^n,$$

and, using the SFE computations above, equate

$$\begin{aligned} \sum_{n=0}^{\infty} \tilde{G}_n[\xi]\delta^n &= \left[\partial_y v - \nabla_x \eta \cdot \nabla_x v\right]_{y=\sigma_\delta} \\ &= \sum_{n=0}^{\infty} \sum_{p\in\Gamma'} (|p| - \nabla_x \eta \cdot (ip)) d_{p,n} e^{ip\cdot x - |p|b + |p|\delta(\eta+b)} \delta^n. \end{aligned}$$

From this we deduce that

$$\tilde{G}_n = \sum_{p\in\Gamma'} \sum_{l=0}^{n} K_{n-l}(|p| - \nabla_x\eta\cdot(ip))e^{-b|p|}\,|p|^{n-l}\,d_{p,l}, \tag{32}$$

where

$$K_l := \frac{(\eta(x)+b)^l}{l!}.$$

Notice that in this computation there is never a need to apply the operator S_D^{-1} and, thus, no need to use the approximating operator B_D^F.

So, our new computational strategy of Stabilized Field Expansions and Dirichlet–Interior Derivative Operators (SFE/DIDO) for computing Dirichlet–Neumann operators amounts to using (31) to compute the coefficients $d_{p,n}$ followed by the utilization of (32) to recover the normal derivative. The computational complexity of these two steps is identical to that of the original FE method (19) & (20), namely $\mathcal{O}(N^2N_x)$, while the storage is merely $\mathcal{O}(NN_x)$. Of course there are two parameters to choose, b and F, which will greatly affect the performance of this new method. For instance, if b is chosen too close to zero then the method will behave much like the FE algorithm and we have achieved nothing new. If b is chosen too large then the "base" for our homotopy will be too far from the surface and we cannot expect good results. It is the subject of current research by Nicholls & Reitich [62], in the setting of electromagnetic and acoustic scattering, to provide guiding principles for the choice of these parameters.

5.3 Numerical Results

In this section we will show some preliminary results to illustrate the effectiveness of our new SFE/DIDO algorithm (§ 5.1 and § 5.2) for computing DNO. For simplicity we will restrict ourselves to the two dimensional setting (periodic on the interval $[0, 2\pi]$) for an ocean of infinite depth ($h = \infty$). For this we will take advantage of a family of exact solutions of the elliptic problem (7) which, for an arbitrary profile $\eta = \varepsilon f$, can be used to specify Dirichlet data and produces *exact* Neumann data. This family of solutions is

$$v_p(x,y) := e^{ip\cdot x+|p|y},$$

for $p \in \Gamma'$, c.f. (13), which, given Dirichlet data,

$$\xi_p(x) := v_p(x,\eta(x)) = e^{ip\cdot x+|p|\eta(x)},$$

produces Neumann data

$$\nu_p(x) := (\partial_y - \nabla_x\eta\cdot\nabla_x)v_p(x,\eta(x)) = (|p| - \nabla_x\eta\cdot(ip))e^{ip\cdot x+|p|\eta(x)}. \tag{33}$$

For all results presented in this section we have set $p = 3$.

We now consider numerical implementations of (19) & (20), which we term the FE method, and (31) & (32), which we denote the SFE/DIDO procedure. For each we will retain N_x Fourier modes and N Taylor coefficients. For each mode $k \in \Gamma'$ in our computation, any Taylor polynomials, e.g.

$$\tau_k(\varepsilon) := \sum_{n=0}^{N} d_{k,n}\varepsilon^n,$$

are summed either directly (Taylor summation) or using Padé approximation (Padé summation) [3, 6, 7, 56].

In these experiments we will consider two interfaces, a "smooth" profile f_s (sinusoidal), and a "rough" profile f_r which is C^4 but not C^5 [58, 59]:

$$f_s(x) = \cos(x), \tag{34a}$$

$$f_r(x) = (2 \times 10^{-4})x^4(2\pi - x)^4 - c_0, , \tag{34b}$$

where c_0 is chosen so that f_r has zero mean. The second of these profiles has an infinite Fourier series representation

$$f_r(x) = \sum_{k=1}^{\infty} \frac{96(2k^2\pi^2 - 1)}{125k^8} \cos(kx),$$

and, in order to minimize the effects of aliasing, we approximate it by its truncated Fourier series:

$$f_{r,P}(x) := \sum_{k=1}^{P} \frac{96(2k^2\pi^2 - 1)}{125k^8} \cos(kx). \tag{35}$$

For the smooth profile f_s, in Figures 13–14 we display the relative error, measured in L^∞, in computing the normal derivative of the field at the boundary, i.e. the DNO, versus perturbation order N. In these simulations we chose $\varepsilon = 0.7$, while the numerical parameters were $N_x = 256$, $N = 60$, $b = 0.0001, 0.01, 1$, and $F = 16$ (Figure 13) or $F = 4$ (Figure 14).

First, we point out the remarkable stabilizing properties which the SFE/DIDO algorithm

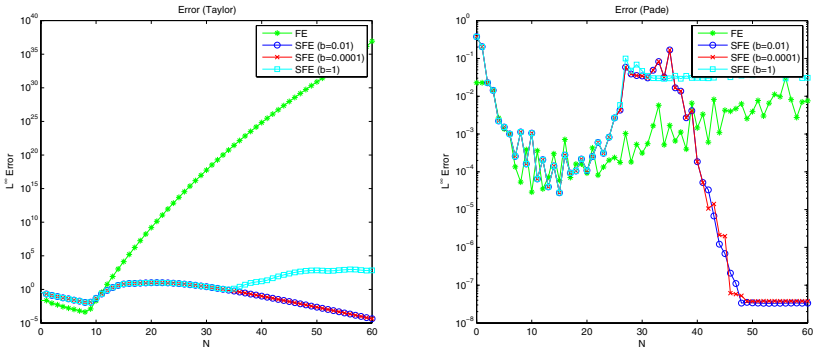

Fig. 13 Relative L^∞ error in FE and SFE/DIDO computations of normal derivative at the boundary for the smooth profile f_s, (34a). Numerical parameters are $N_x = 256$, $N = 60$, $b = 0.0001, 0.01, 1$, $F = 16$. For the calculation depicted on the left Taylor summation is utilized, while for that on the right Padé summation is used.

possesses: The FE algorithm begins to diverge at $N = 9$ while the enhanced summation of Padé approximation can only ever deliver accuracy of 10^{-4}. However, our new SFE/DIDO procedure produces solutions which are increasingly more accurate throughout *all* orders, though they can be disadvantaged when b is chosen as large as one. Interestingly, the reduction

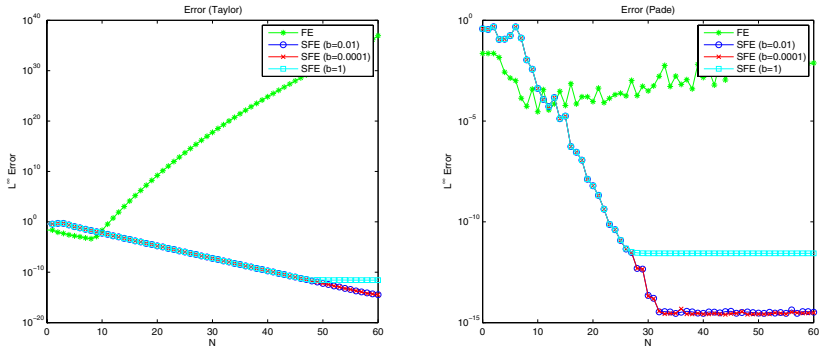

Fig. 14 Relative L^∞ error in FE and SFE/DIDO computations of normal derivative at the boundary for the smooth profile f_s, (34a). Numerical parameters are $N_x = 256$, $N = 60$, $b = 0.0001, 0.01, 1$, $F = 4$. For the calculation depicted on the left Taylor summation is utilized, while for that on the right Padé summation is used.

in the "operator filter" F has the effect of producing slightly worse results for N small, while producing results which are drastically better for N large; for instance, SFE/DIDO reaches only 10^{-8} accuracy when $F = 16$, while it achieves full double precision accuracy when $F = 4$ (provided, in these experiments, that $b < 1$).

Finally, for the rough profile f_r^P, we display in Figures 15–16 the relative error, measured in L^∞, in computing the DNO versus perturbation order N. In this simulation we again choose $\varepsilon = 0.7$, while the numerical parameters were $N_x = 256$, $N = 60$, $b = 0.0001, 0.01, 1$, $P = 40$, and $F = 16$ (Figure 15) or $F = 4$ (Figure 16). Again, we point out the stable

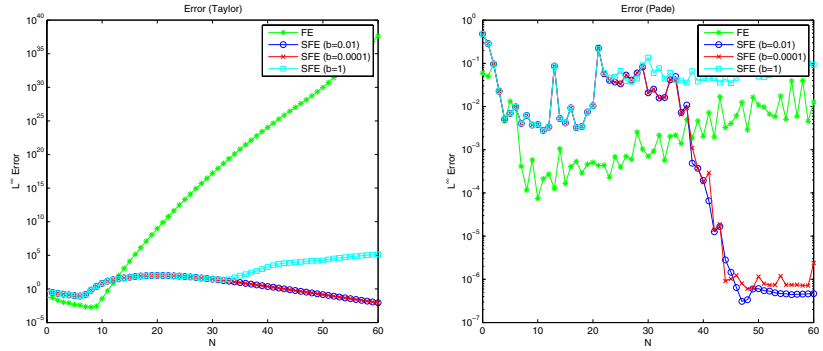

Fig. 15 Relative L^∞ error in FE and SFE/DIDO computations of normal derivative at the boundary for the rough profile f_r^{40}, (35). Numerical parameters are $N_x = 256$, $N = 60$, $b = 0.0001, 0.01, 1$, $F = 16$. For the calculation depicted on the left Taylor summation is utilized, while for that on the right Padé summation is used.

nature of the SFE/DIDO method, which produces consistently improved answers throughout all perturbation orders. Again, this effect is largely independent of the parameter b, though $b = 1$ is clearly disadvantaged in this case. Again, the role of F is significant and it is clear

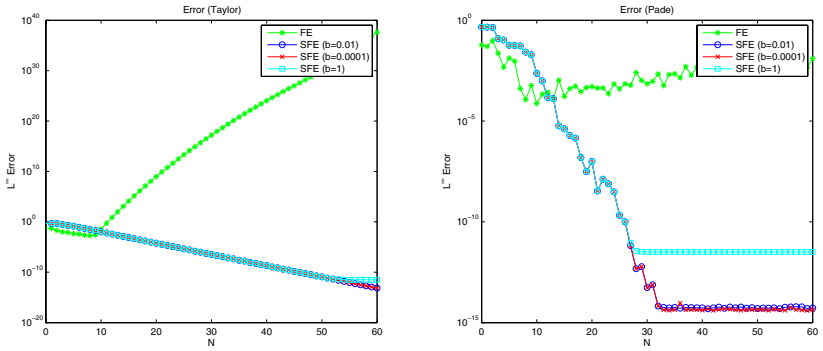

Fig. 16 Relative L^∞ error in FE and SFE/DIDO computations of normal derivative at the boundary for the rough profile f_r^{40}, (35). Numerical parameters are $N_x = 256$, $N = 60$, $b = 0.0001, 0.01, 1$, $F = 4$. For the calculation depicted on the left Taylor summation is utilized, while for that on the right Padé summation is used.

that future research [62] is necessary to not only provide guidance on the choice of b and F, but also give an explanation for the behavior of this new algorithm.

Acknowledgements The author gratefully acknowledges support from the NSF through grant No. DMS–0537511.

References

[1] Mark J. Ablowitz and Harvey Segur. *Solitons and the inverse scattering transform*, volume 4 of *SIAM Studies in Applied Mathematics*. Society for Industrial and Applied Mathematics (SIAM), Philadelphia, Pa., 1981.

[2] Eugene L. Allgower and Kurt Georg. *Numerical continuation methods*. Springer-Verlag, Berlin, 1990.

[3] George A. Baker, Jr. and Peter Graves-Morris. *Padé approximants*. Cambridge University Press, Cambridge, second edition, 1996.

[4] J. Thomas Beale. A convergent boundary integral method for three-dimensional water waves. *Math. Comp.*, 70(235):977–1029, 2001.

[5] Oscar P. Bruno and Fernando Reitich. Numerical solution of diffraction problems: A method of variation of boundaries. *J. Opt. Soc. Am. A*, 10(6):1168–1175, 1993.

[6] Oscar P. Bruno and Fernando Reitich. Numerical solution of diffraction problems: A method of variation of boundaries. II. Finitely conducting gratings, Padé approximants, and singularities. *J. Opt. Soc. Am. A*, 10(11):2307–2316, 1993.

[7] Oscar P. Bruno and Fernando Reitich. Numerical solution of diffraction problems: A method of variation of boundaries. III. Doubly periodic gratings. *J. Opt. Soc. Am. A*, 10(12):2551–2562, 1993.

[8] Oscar P. Bruno and Fernando Reitich. Calculation of electromagnetic scattering via boundary variations and analytic continuation. *Appl. Comput. Electromagn. Soc. J.*, 11(1):17–31, 1996.

[9] Oscar P. Bruno and Fernando Reitich. Boundary–variation solutions for bounded–obstacle scattering problems in three dimensions. *J. Acoust. Soc. Am.*, 104(5):2579–2583, 1998.

[10] Oscar P. Bruno and Fernando Reitich. High-order boundary perturbation methods. In *Mathematical Modeling in Optical Science*, volume 22, pages 71–109. SIAM, Philadelphia, PA, 2001. Frontiers in Applied Mathematics Series.
[11] P. J. Bryant. Doubly periodic progressive permanent waves in deep water. *J. Fluid Mech.*, 161:27–42, 1985.
[12] A. P. Calderón. Cauchy integrals on Lipschitz curves and related operators. *Proc. Nat. Acad. Sci. USA*, 75:1324–1327, 1977.
[13] Claudio Canuto, M. Yousuff Hussaini, Alfio Quarteroni, and Thomas A. Zang. *Spectral methods in fluid dynamics*. Springer-Verlag, New York, 1988.
[14] R. Coifman and Y. Meyer. Nonlinear harmonic analysis and analytic dependence. In *Pseudodifferential operators and applications (Notre Dame, Ind., 1984)*, pages 71–78. Amer. Math. Soc., 1985.
[15] W. Craig, C. Sulem, and P.-L. Sulem. Nonlinear modulation of gravity waves: a rigorous approach. *Nonlinearity*, 5(2):497–522, 1992.
[16] Walter Craig. An existence theory for water waves and the Boussinesq and Korteweg-de Vries scaling limits. *Comm. Partial Differential Equations*, 10(8):787–1003, 1985.
[17] Walter Craig. Birkhoff normal forms for water waves. In *Mathematical problems in the theory of water waves (Luminy, 1995)*, volume 200 of *Contemp. Math.*, pages 57–74. Amer. Math. Soc., Providence, RI, 1996.
[18] Walter Craig and Mark D. Groves. Hamiltonian long-wave approximations to the water-wave problem. *Wave Motion*, 19(4):367–389, 1994.
[19] Walter Craig and Mark D. Groves. Normal forms for wave motion in fluid interfaces. *Wave Motion*, 31(1):21–41, 2000.
[20] Walter Craig, Philippe Guyenne, Joe Hammack, Diane Henderson, and Catherine Sulem. Solitary wave interactions. *Phys. Fluids*, 18:057106, 2006.
[21] Walter Craig, Philippe Guyenne, and Henrik Kalisch. Hamiltonian long-wave expansions for free surfaces and interfaces. *Comm. Pure Appl. Math.*, 58(12):1587–1641, 2005.
[22] Walter Craig, Philippe Guyenne, David P. Nicholls, and Catherine Sulem. Hamiltonian long wave expansions for water waves over a rough bottom. *Proc. Roy. Soc. Lond., A*, 461(2055):839–873, 2005.
[23] Walter Craig and David P. Nicholls. Traveling two and three dimensional capillary gravity water waves. *SIAM J. Math. Anal.*, 32(2):323–359, 2000.
[24] Walter Craig and David P. Nicholls. Traveling gravity water waves in two and three dimensions. *Eur. J. Mech. B Fluids*, 21(6):615–641, 2002.
[25] Walter Craig, Ulrich Schanz, and Catherine Sulem. The modulation regime of three-dimensional water waves and the Davey-Stewartson system. *Ann. Inst. Henri Poincaré*, 14:615–667, 1997.
[26] Walter Craig and Catherine Sulem. Numerical simulation of gravity waves. *Journal of Computational Physics*, 108:73–83, 1993.
[27] Walter Craig and Patrick A. Worfolk. An integrable normal form for water waves in infinite depth. *Phys. D*, 84(3-4):513–531, 1995.
[28] Michael G. Crandall and Paul H. Rabinowitz. Bifurcation from simple eigenvalues. *J. Functional Analysis*, 8:321–340, 1971.
[29] R. de la Llave and P. Panayotaros. Gravity waves on the surface of the sphere. *J. Nonlinear Sci.*, 6(2):147–167, 1996.
[30] Frédéric Dias and Christian Kharif. Nonlinear gravity and capillary-gravity waves. In *Annual review of fluid mechanics, Vol. 31*, pages 301–346. Annual Reviews, Palo Alto, CA, 1999.
[31] Douglas G. Dommermuth and Dick K. P. Yue. A high-order spectral method for the study of nonlinear gravity waves. *Journal of Fluid Mechanics*, 184:267–288, 1987.
[32] Lawrence C. Evans. *Partial differential equations*. American Mathematical Society, Providence, RI, 1998.
[33] J. D. Fenton and M. M. Rienecker. A Fourier method for solving nonlinear water-wave problems: application to solitary-wave interactions. *J. Fluid Mech.*, 118:411–443, 1982.

[34] David Gottlieb and Steven A. Orszag. *Numerical analysis of spectral methods: theory and applications*. Society for Industrial and Applied Mathematics, Philadelphia, Pa., 1977. CBMS-NSF Regional Conference Series in Applied Mathematics, No. 26.
[35] S.T. Grilli, P. Guyenne, and F. Dias. A fully nonlinear model for three-dimensional overturning waves over an arbitrary bottom. *Int. J. Numer. Meth. Fluids*, 35:829–867, 2001.
[36] Philippe Guyenne and David P. Nicholls. Numerical simulation of solitary waves on plane slopes. *Math. Comput. Simul.* 69:269–281,2005.
[37] Joe Hammack and Diane Henderson. Experiments on deep–water waves with two–dimensional surface patterns. In *Proceedings of the 21st International Conference on Offshore Mechanics and Arctic Engineering, Oslo, Norway, 23-28 June 2002*, 2002.
[38] Joe Hammack, Diane Henderson, and Harvey Segur. Progressive–water waves with persistent two–dimensional surface patterns. *J. Fluid. Mech.*, 532:1–52, 2005.
[39] Bei Hu and David P. Nicholls. Analyticity of Dirichlet–Neumann operators on Hölder and Lipschitz domains. *SIAM J. Math. Anal.*, 37(1):302–320, 2005.
[40] Tadayoshi Kano and Takaaki Nishida. Une justification mathématique pour l'équation de Korteweg-de Vries approchant des ondes longues de surface de l'eau. *Proc. Japan Acad. Ser. A Math. Sci.*, 61(10):345–348, 1985.
[41] Tadayoshi Kano and Takaaki Nishida. A mathematical justification for Korteweg-de Vries equation and Boussinesq equation of water surface waves. *Osaka J. Math.*, 23(2):389–413, 1986.
[42] H. B. Keller. *Lectures on numerical methods in bifurcation problems*. Published for the Tata Institute of Fundamental Research, Bombay, 1987.
[43] Horace Lamb. *Hydrodynamics*. Cambridge University Press, Cambridge, sixth edition, 1993.
[44] David Lannes. Well-posedness of the water-waves equations. *J. Amer. Math. Soc.*, 18(3):605–654 (electronic), 2005.
[45] T. Levi-Civita. Détermination rigoureuse des ondes permanentes d'ampleur finie. *Math. Ann.*, 93:264–314, 1925.
[46] Yuming Liu, Ming Xue, and Dick K. P. Yue. Computations of fully nonlinear three-dimensional wave-wave and wave-body interactions. II. Nonlinear waves and forces on a body. *J. Fluid Mech.*, 438:41–66, 2001.
[47] T. R. Marchant and A. J. Roberts. Properties of short-crested waves in water of finite depth. *J. Austral. Math. Soc. Ser. B*, 29(1):103–125, 1987.
[48] D. Meiron, P. Saffman, and H. Yuen. Calculation of steady three-dimensional deep-water waves. *Journal of Fluid Mechanics*, 124:109+, 1982.
[49] D. Michael Milder. The effects of truncation on surface-wave Hamiltonians. *J. Fluid Mech.*, 217:249–262, 1990.
[50] David P. Nicholls. *Traveling Gravity Water Waves in Two and Three Dimensions*. PhD thesis, Brown University, 1998.
[51] David P. Nicholls. Traveling water waves: Spectral continuation methods with parallel implementation. *J. Comput. Phys.*, 143(1):224–240, 1998.
[52] David P. Nicholls. On hexagonal gravity water waves. *Math. Comput. Simul.*, 55(4–6):567–575, 2001.
[53] David P. Nicholls and Nilima Nigam. Exact non-reflecting boundary conditions on general domains. *J. Comput. Phys.*, 194(1):278–303, 2004.
[54] David P. Nicholls and Nilima Nigam. Error analysis of an enhanced DtN-FE method for exterior scattering problems. *Numerische Mathematik*, 105(2):267–298, 2006.
[55] David P. Nicholls and Fernando Reitich. A new approach to analyticity of Dirichlet-Neumann operators. *Proc. Roy. Soc. Edinburgh Sect. A*, 131(6):1411–1433, 2001.
[56] David P. Nicholls and Fernando Reitich. Stability of high-order perturbative methods for the computation of Dirichlet-Neumann operators. *J. Comput. Phys.*, 170(1):276–298, 2001.
[57] David P. Nicholls and Fernando Reitich. Analytic continuation of Dirichlet-Neumann operators. *Numer. Math.*, 94(1):107–146, 2003.

[58] David P. Nicholls and Fernando Reitich. Shape deformations in rough surface scattering: Cancellations, conditioning, and convergence. *J. Opt. Soc. Am. A*, 21(4):590–605, 2004.
[59] David P. Nicholls and Fernando Reitich. Shape deformations in rough surface scattering: Improved algorithms. *J. Opt. Soc. Am. A*, 21(4):606–621, 2004.
[60] David P. Nicholls and Fernando Reitich. On analyticity of traveling water waves. *Proc. Roy. Soc. Lond., A*, 461(2057):1283–1309, 2005.
[61] David P. Nicholls and Fernando Reitich. Rapid, stable, high–order computation of traveling water waves in three dimensions. *Eur. J. Mech. B Fluids*, 25(4):406–424, 2006.
[62] David P. Nicholls and Fernando Reitich. Stable, rapid boundary perturbation algorithms for direct scattering: The two dimensional case. *in preparation*, 2006.
[63] David P. Nicholls and Mark Taber. Joint analyticity and analytic continuation for Dirichlet–Neumann operators on doubly perturbed domains. *J. Fluid Mech. (to appear)*, 2007.
[64] J. Reeder and M. Shinbrot. On Wilton ripples II: Rigorous results. *Arch. Rat. Mech. Anal.*, 77:321–347, 1981.
[65] J. Reeder and M. Shinbrot. Three dimensional nonlinear wave interaction in water of constant depth. *Nonlinear Analysis*, 5:303–323, 1981.
[66] John Reeder and Marvin Shinbrot. The initial value problem for surface waves under gravity. II. The simplest 3-dimensional case. *Indiana Univ. Math. J.*, 25(11):1049–1071, 1976.
[67] John Reeder and Marvin Shinbrot. The initial value problem for surface waves under gravity. III. Uniformly analytic initial domains. *J. Math. Anal. Appl.*, 67(2):340–391, 1979.
[68] John Reeder and Marvin Shinbrot. On Wilton ripples. I. Formal derivation of the phenomenon. *Wave Motion*, 3(2):115–135, 1981.
[69] M. M. Rienecker and J. D. Fenton. A Fourier approximation method for steady water waves. *J. Fluid Mech.*, 104:119–137, 1981.
[70] A. J. Roberts. Highly nonlinear short-crested water waves. *J. Fluid Mech.*, 135:301–321, 1983.
[71] A. J. Roberts and D. H. Peregrine. Notes on long-crested water waves. *J. Fluid Mech.*, 135:323–335, 1983.
[72] A. J. Roberts and L. W. Schwartz. The calculation of nonlinear short-crested gravity waves. *Phys. Fluids*, 26:2388–2392, 1983.
[73] P. G. Saffman and H. C. Yuen. Three-dimensional waves on deep water. In *Advances in nonlinear waves, Vol. II*, pages 1–30. Pitman, Boston, Mass., 1985.
[74] Ulrich Schanz. *On the Evolution of Gravity-Capillary Waves in Three Dimensions*. PhD thesis, University of Toronto, 1997.
[75] L. W. Schwartz. Computer extension and analytic continuation of Stokes' expansion for gravity waves. *J. Fluid Mech.*, 62:553–578, 1974.
[76] Leonard W. Schwartz and Jean-Marc Vanden-Broeck. Numerical solution of the exact equations for capillary-gravity waves. *J. Fluid Mech.*, 95(1):119–139, 1979.
[77] Marvin Shinbrot. The initial value problem for surface waves under gravity. I. The simplest case. *Indiana Univ. Math. J.*, 25(3):281–300, 1976.
[78] Ralph A. Smith. An operator expansion formalism for nonlinear surface waves over variable depth. *J. Fluid Mech.*, 363:333–347, 1998.
[79] D. Struik. Détermination rigoureuse des ondes irrotationnelles périodiques dans un canal à profondeur finie. *Math. Ann.*, 95:595–634, 1926.
[80] Wu-Ting Tsai and Dick K. P. Yue. Computation of nonlinear free-surface flows. In *Annual review of fluid mechanics, Vol. 28*, pages 249–278. Annual Reviews, Palo Alto, CA, 1996.
[81] Kenneth M. Watson and Bruce J. West. A transport–equation description of nonlinear ocean surface wave interactions. *Journal of Fluid Mechanics*, 70:815–826, 1975.
[82] B. J. West, K. A. Brueckner, R. S. Janda, D. M. Milder, and R. L. Milton. A new numerical method for surface hydrodynamics. *J. Geophys. Res.*, 92:11803–11824, 1987.
[83] Sijue Wu. Well-posedness in Sobolev spaces of the full water wave problem in 2-D. *Invent. Math.*, 130(1):39–72, 1997.

[84] Sijue Wu. Well-posedness in Sobolev spaces of the full water wave problem in 3-D. *J. Amer. Math. Soc.*, 12(2):445–495, 1999.

[85] Ming Xue, Hongbo Xü, Yuming Liu, and Dick K. P. Yue. Computations of fully nonlinear three-dimensional wave-wave and wave-body interactions. I. Dynamics of steep three-dimensional waves. *J. Fluid Mech.*, 438:11–39, 2001.

[86] Vladimir Zakharov. Stability of periodic waves of finite amplitude on the surface of a deep fluid. *Journal of Applied Mechanics and Technical Physics*, 9:190–194, 1968.